

Experimental observation of vortex gyrotropic mode excited by surface acoustic waves

R. Lopes Seeger,^{1,2*} F. Millo,¹ G. Soares,² J.-V. Kim,¹ A. Solignac,² G. de Loubens,² and T. Devolder¹

¹Centre de Nanosciences et de Nanotechnologies, CNRS, Université Paris-Saclay, 91120, Palaiseau, France

²SPEC, CEA, CNRS, Université Paris-Saclay, 91191 Gif-sur-Yvette, France

*To whom correspondence should be addressed; E-mail: rafael.lopes-seeger@c2n.upsaclay.fr.

(Dated: October 2, 2024)

arXiv:2409.05998v2 [cond-mat.mtrl-sci] 1 Oct 2024

Abstract

The traditional method for exciting spin-wave dynamics in magnetic materials involves microwave magnetic fields generated by current injection into inductive antennas. However, there is a growing interest in non-inductive excitation methods. Magneto-acoustic effects present a viable alternative, where strains produced by applying voltages to a piezoelectric substrate can couple to spin-waves in a magnetic film. Recently, it has been proposed that surface acoustic waves (SAWs) can excite the gyrotropic mode of the vortex state in a magnetic disk. Here we report on experiments utilizing a magnetic resonance force microscope to investigate magnetization dynamics in CoFeB sub-micrometer disks in the vortex state, grown on a Z-cut LiNbO₃ substrate. The device design enables excitation of the gyrotropic mode either inductively, using an antenna on top of the disks, or acoustically via SAWs launched from an interdigital transducer. Our modelling indicates that the lattice rotation ω_{xz} generates a localized magneto-acoustic field that displaces the vortex core from the disk center, initiating the gyration motion. Tuning of the magneto-acoustic torque acting on the vortex structure is achieved by a perpendicular magnetic field. These results offer valuable insights into the excitation of vortex gyration by magneto-acoustic excitation and open up new possibilities for designing functional devices in spintronics and magnonics by leveraging a mechanism that is effective in all magnetic materials.

INTRODUCTION

The study of the magnetization dynamics driven by surface acoustic waves (SAWs) has seen significant progress over the past decade [1–5]. This emerging field holds promise for the development of integrated microwave devices that leverage the advantages of magnonics and microwave acoustics. SAWs are widely used for delaying and filtering of radio frequency signals. Additionally, SAWs can excite spin-waves (SWs) in magnetic films, which turns out to be a fertile playground for realizing acoustic isolators based on SAWs nonreciprocity. These applications rely on the variety of underlying SAW-SW interaction mechanisms and high tunability of the magnetic system [6–10]. While the use of SAWs to excite magnetization dynamics was initially limited to ferromagnets, recent advancements have extended its applicability to multiferroics [11], synthetic antiferromagnets [12], and layered antiferromagnets [13].

A particularly interesting example of magnetization dynamics is found in magnetic vortices. These inhomogeneous magnetic textures can be formed in magnetic disks of specific aspect ratios, featuring in-plane magnetization curling along the disk’s perimeter and out-of-plane magnetization at the center, which defines the vortex core [14, 15]. At remanence the vortex core is localized at the center of the disk. Resonant excitation by a microwave field induces a gyrotropic dynamics of the vortex core about its equilibrium position [15, 16]. Furthermore, vortex gyrotropic dynamics can also be triggered by a spin-polarized current through spin-transfer torque [17, 18]. There is a strong interest in achieving excitation through non-inductive methods due to the absence of currents flowing through the device, and a promising approach involves using

SAWs for strain-driven magnetization dynamics [19]. Recent simulations indicate that longitudinal strain (ϵ_{xx}) produces an effective field of magneto-elastic origin ('tickle' field) that can drive the gyrotropic mode, but only when an in-plane magnetic field is applied, displacing the vortex core from the disk's center [19]. At zero applied field, the resulting anti-symmetric magneto-acoustic field across the vortex structure does not excite gyration dynamics because it averages to zero. It is noteworthy that in real piezoelectric materials there are additional non-zero lattice deformation components that may have different symmetry properties compared to the magneto-elastic effect of only the longitudinal strain [20, 21]. In particular, the rotational motion of the lattice within the magnetic material causes reorientation of the surface normal direction, which couples to the magnetization via magnetic anisotropy fields [22]. Notably, the so called magneto-rotation contribution ('rolling' field) is active in materials with vanishing magnetostriction.

In this study, we discuss experimental results on propagating SAWs in a magnetostrictive disk hosting a vortex. Figure 1(A) shows a schematic illustration of the experimental setup. The vortex core dynamics is excited by the effective magneto-acoustic field associated to oscillation of the lattice. A perpendicular magnetic field is applied to tune the gyrotropic frequency [23]. When the SAW frequency matches the vortex gyrotropic frequency for a given applied field, the magneto-acoustic field leads to a resonant excitation of the gyration dynamics. To elucidate the origin of this phenomenon, we extend the previous model by taking into account the lattice rotation ω_{xz} of elastic deformation $\omega_{ij} = \frac{1}{2} \left(\frac{\partial u_i}{\partial x_j} - \frac{\partial u_j}{\partial x_i} \right)$, where $u_i, i = x, y, z$ are the components of the lattice displacement. This turns out to be crucial as it induces a net in-plane rolling field which is highly localized near the vortex core. Such an effective field expels the vortex core away from the disk center and can be efficiently used for the resonant excitation of the vortex core gyration. The gyration trajectories are inflated by the application of a perpendicular magnetic field due to enhanced magneto-acoustic torque acting on the canted vortex texture.

RESULTS

Gyrotropic excitation of magnetic vortex

Figure 1(A) illustrates the schematics of a SAW propagation through a CoFeB disk positioned on a piezoelectric substrate, specifically Z-cut LiNbO₃. The CoFeB disk has a thickness $t_{\text{FM}} = 34$ nm and a diameter $2R = 800$ nm. SAWs, with a wavelength of $4.5 \mu\text{m}$ corresponding to the 2nd harmonic order, are generated by an interdigital transducer (IDT of periodicity $9 \mu\text{m}$) and propagate on the surface of the piezoelectric substrate, exciting the vortex gyrotropic mode within the magnetic disk. The SAWs propagate along the crystalline X-axis of LiNbO₃, which coincides with the x -axis shown in Fig. 1(A). The disk is

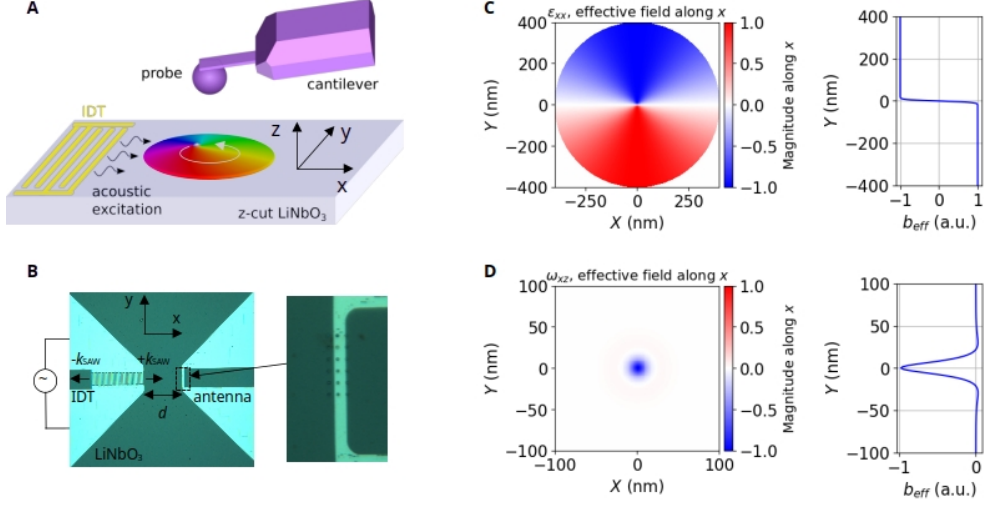


FIG. 1. Vortex gyration induced by SAWs. (A) Sketch of the experiments employing an IDT to excite SAWs, which propagate on the surface of the piezoelectric substrate towards a disk in the vortex state (the colors encode the in-plane magnetization component). The detection of magnetization dynamics is achieved using MRFM. In addition to the IDT, the device comprises a top inductive antenna that allows inductive excitation, as shown in the optical image (B), where the inset is a zoomed view of the antenna's constriction with several CoFeB microdisks. Normalized magneto-acoustic fields (b_{eff}) distribution over the vortex in the absence of an applied field corresponding to a (C) tickle field associated with the lattice strain ϵ_{xx} and rolling field associated to a (D) rotation ω_{xz} . The color codes indicate the effective magneto-acoustic field in the x -direction.

placed $d = 104 \mu\text{m}$ away from the IDT. As the SAWs travel beneath the magnetic vortex, the oscillation of the lattice induces an effective magnetic field through magneto-elastic and magneto-rotation coupling mechanisms. Alternatively, the magnetization dynamics can be excited by a microwave field generated via an inductive antenna placed on top of the disk (antenna width $w_{\text{ant}} = 4 \mu\text{m}$, Fig. 1(B)). To detect the magnetization dynamics in single magnetic vortex disks, we utilize a magnetic resonance force microscope (MRFM) [23, 24]. Further details on sample fabrication and MRFM are provided in the Methods section.

We initially perform the MRFM spectroscopy of the magnetic vortex when excited by an in-plane microwave field generated via the inductive antenna [Fig. 2(A)]. By sweeping the amplitude of the perpendicular magnetic field at fixed microwave frequency, we observe an erratic variation of the gyration frequency of the vortex, ranging from 0.4 to 1.2 GHz, instead of the expected linear variation [23], from $\omega_G(H_z = 0)/(2\pi) = 5/(9\pi)\gamma\mu_0 M_s(t/R) \simeq 0.72 \text{ GHz}$ to $\omega_G(H_z = H_{\text{sat}})/(2\pi) \simeq 1.44 \text{ GHz}$. $H_{\text{sat}} \simeq M_s$ is the saturation field of the disk, $\mu_0 M_s \simeq 1.7 \text{ T}$ the CoFeB saturation magnetization, and $\gamma/(2\pi) \simeq 28 \text{ GHz/T}$ its gyrotropic ratio. Similar MRFM spectroscopy results, obtained on another CoFeB disk, are presented in the supplementary material. This behavior is attributed to the strong pinning of the vortex core to grain defects

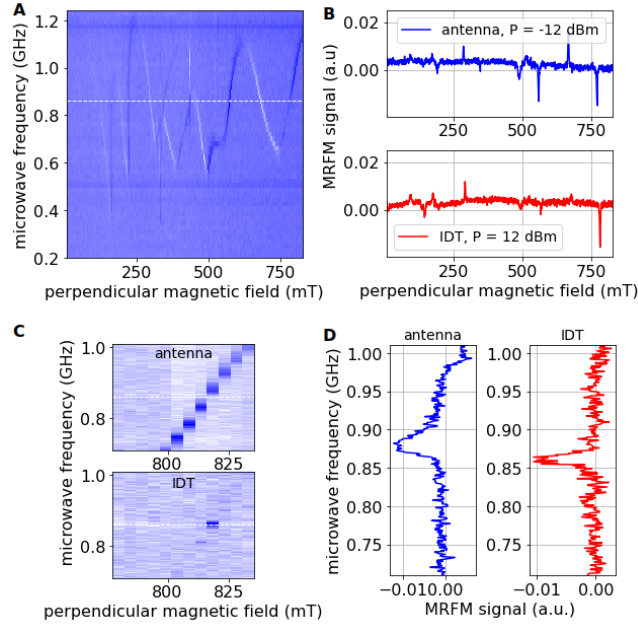


FIG. 2. Comparison of vortex gyrotropic excitation employing microwave inductive and magneto-acoustic fields. (A) Dependence of vortex gyration frequency on the perpendicular magnetic field probed using the broadband inductive antenna. The contrast corresponds to the MRFM signal amplitude. (B) Gyrotropic spectroscopy as function of perpendicular field with the microwave signal applied either to the antenna or the IDT. The fixed excitation frequency of 0.86 GHz, indicated by the horizontal line in (A), corresponds to the 2nd harmonics of SAW generated by the IDT. (C) f -scans comparing the inductive and acoustic excitations of vortex gyration. (D) Gyration signal as function of f at a fixed field of 820 mT.

in the CoFeB disk. The phenomenon of vortex core pinning and its influence on the gyration frequency has been extensively studied in previous works [25, 26]. In Fig. 2(B), we compare the MRFM spectrum of the vortex gyration induced by the microwave field from the antenna with the one generated by the effective magneto-acoustic field from the SAW excitation by the IDT. The microwave frequency is fixed to 0.86 GHz, corresponding to the second harmonic of acoustic waves resonantly excited by applying an rf voltage on the IDT (see supplemental material). The gyrotropic response of the vortex displays the same spectrum in the two cases, albeit with distinct relative amplitudes between the resonant features, a signature of the distinct mechanisms by which the inductive microwave field and SAW couple to the vortex dynamics in the disk.

We also performed frequency(f)-dependent measurements employing either the antenna or the IDT [see Fig. 2(C,D)]. They clearly illustrate that the excitation of the vortex gyrotropic mode by acoustic waves is only effective at the resonance of the IDT with SAWs, contrary to the broadband excitation provided by the inductive antenna. In fact, there is no excitation of the vortex core at $f \neq 0.86$ GHz due to the large detuning between the SAW resonance and the vortex gyration frequency. In addition, the frequency width of the IDT

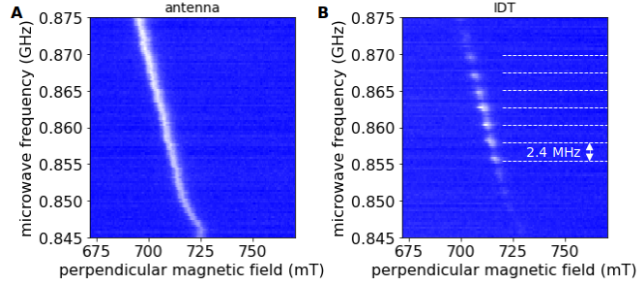


FIG. 3. High frequency resolution gyrotropic spectroscopy. Perpendicular magnetic field dependence for an excitation employing the antenna (A) or the IDT (B). In the latter case, oscillations with a period of ≈ 2.4 MHz appear due to standing acoustic modes in the LiNbO_3 substrate, see discussion in the text.

signal is less than the one using the antenna, 15.7 and 30.9 MHz, respectively. This is the case because the linewidth is not determined by the gyrotropic response of the CoFeB disk, but by the SAW resonance, that is narrower. This proves that the mechanisms to excite the gyrotropic mode in the two cases are distinct, and that the signal detected when using the IDT excitation is originating from the magneto-acoustic torques.

Fine structure of the SAW excitation

To gain further insight into the observed signal, we performed high frequency resolution experiments around the SAW resonance at 0.86 GHz, as shown in Fig. 3. For the IDT excitation, strong oscillations of the MRFM signal amplitude are observed, in contrast to the antenna excitation where it remains almost constant over the full frequency range. These oscillations are due to standing acoustic modes formed along the SAW propagation direction caused by the reflection from the edge of the substrate [27]. The SAWs emitted by the IDT that travel along the LiNbO_3 surface can indeed propagate over millimeter distances [28]. The sample length along the SAW propagation direction is approximately $\ell = 1.8$ mm, which for the typical SAW velocity ($v = 3900$ m/s) in LiNbO_3 results in a frequency splitting v/ℓ of around 2.2 MHz between consecutive standing modes, in good agreement with the oscillation period observed in Fig. 3(B) (see supplementary material for additional experiments of this kind in a different range of fields).

The corollary of the existence of standing acoustic modes is that the elastic power injected by the IDT is effectively spread over the entire length ℓ of the substrate, in stark contrast with the much more localized power of the microwave field of the inductive antenna. The observation of such a fine structure in the SAW signal unambiguously points towards the acoustic origin of the vortex gyration induced by the IDT excitation.

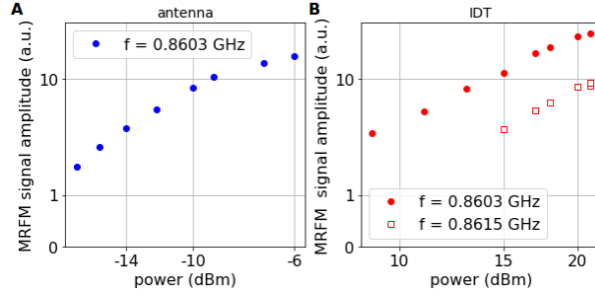


FIG. 4. MRFM signal amplitude as function of the excitation power. Logarithmic-scale dependence as measured with (A) inductive and (B) acoustic excitation as measured for different microwave frequencies. The experiments are performed in the same range of perpendicular field as in Fig. 3.

Power dependence

Finally, we explore the magnitude of the effective excitation field generated by the magneto-acoustic coupling. Figure 4 compares the input power(P)-dependence of the MRFM signal amplitude with inductive and acoustic excitations (see supplementary material for the corresponding raw data). As P increases, the gyration signal increases monotonically. At low excitation powers, a symmetric resonance peak is observed. This behaviour is typical for the linear dynamics regime. In contrast, at higher powers, the peak becomes distorted exhibiting signs of nonlinear dynamics, as reported in previous works [29, 30]. The signal amplitude comparison (Fig. 4) indicates that the propagating SAWs can also generate an effective field capable of exciting large precession amplitudes, however at the cost of 24 dB higher electrical power. This apparently large number is actually another illustration of the much higher efficiency of the magneto-acoustic method compared to the inductive one. A fair comparison between them should indeed take into account the ratio between the volumes hosting significant amplitudes of elastic deformations and microwave fields, which can be evaluated by $20 \log_{10}(\ell/w_{\text{ant}}) \approx 53$ dB.

Micromagnetic simulations: acoustic driven gyrotropic mode

To understand why the gyrotropic dynamics is excited without needing to displace the vortex core from the disk's center with the help of an in-plane magnetic field, we performed micromagnetic simulations [31]. The SAWs that excite the magnetization dynamics in the CoFeB disks are represented by a plane wave with frequency f and deformation amplitude A_{SAW} for the strain components ϵ_{xx} and ϵ_{zz} , as well as for the rotation component ω_{xz} . Those are the non-zero lattice strain and rotation components of a Rayleigh SAW travelling in an isotropic substrate mimicking [21] the Z-cut of LiNbO₃. We stress the fact that the shear

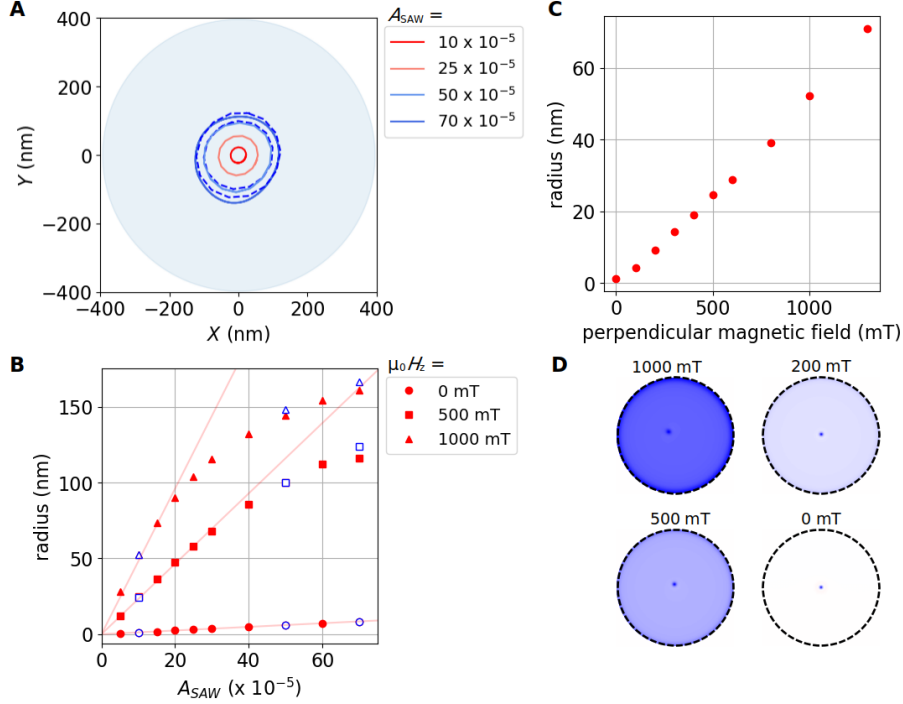


FIG. 5. Micromagnetic simulations. (A) Vortex core trajectories for selected deformation amplitudes A_{SAW} considering the strain components ϵ_{xx} and ϵ_{zz} , and rotation component ω_{xz} at the gyrotropic frequency, with $\mu_0 H_z = 500$ mT. The bold lines are the trajectories driven by ϵ_{xx} , ϵ_{zz} , and ω_{xz} components, while the dashed lines are the trajectories considering only ω_{xz} component. (B) Trajectory radius as function of A_{SAW} for different applied fields. The open symbols represents the trajectories considering the effect of ω_{xz} alone. (C) Trajectory radius as function of the applied field $\mu_0 H_z$ and for $A_{SAW} = 10 \times 10^{-5}$. (D) Normalized rolling fields distribution over the vortex structure with different applied fields. The dashed circles indicate the disk edge.

strain ϵ_{xz} exactly vanishes at the surface between the piezoelectric substrate and the magnetic disk. More details on the simulations are provided in the Methods section.

We first investigate the effect of only the longitudinal strain. As discussed in Ref. [19], ϵ_{xx} alone cannot drive the gyrotropic mode, which we confirm by our calculation of the profile of the tickle field, which exhibits an anti-symmetric distribution [Fig. 1(C)]. As already pointed out in [19], one possibility to work around this problem is to apply an in-plane magnetic field to displace the vortex core away from the disk center in the transverse direction. By symmetry considerations, such an in-plane field basically breaks the axial symmetry of the static vortex, allowing the coupling of the gyrotropic mode to the magneto-acoustic field [19, 32].

There is an alternative way to initiate the vortex core dynamics. As shown in Fig. 1(D) the spatial average of the effective rolling field arising from ω_{xz} is not vanishing. Despite its highly localized character near

the vortex core, it couples to the gyrotropic mode. This net in-plane effective field deriving the magneto-rotation coupling has also been calculated in Ref. [20]. Therefore, it provides a mechanism to drive the vortex gyrotropic mode even from the centered equilibrium position of the core.

Vortex core trajectories

Having discussed the mechanism that starts the vortex motion, we now consider SAWs travelling along the x -axis for further simulations. We will see that in addition to initiating the vortex motion, the lattice rotation alone is capable of maintaining stable gyrotropic motion. We analyse the vortex core motion around its equilibrium position in response to the effective magneto-acoustic field. The non-vanishing components of the lattice deformation are the ϵ_{xx} and ϵ_{zz} of the strain tensor and the rotation ω_{xz} . We emphasize that no gyration is observed when the vortex core is excited by only the ϵ_{xx} and ϵ_{zz} components, without the ω_{xz} component. The gyration motion of the observed magnetization excitation is confirmed by visualizing the vortex core trajectories at resonance for a given deformation amplitude and out-of-plane magnetic field. Fig. 5(A) shows the trajectories for selected values of A_{SAW} , with $\mu_0 H_z = 500$ mT. For moderate deformation amplitudes the vortex core trajectory is circular, while for high A_{SAW} values, it is distorted and becomes non-circular. For comparison, the dashed line in Fig. 5(A) shows the circular trajectory as obtained considering solely the ω_{xz} component for $A_{\text{SAW}} = 50 \times 10^{-5}$ and 70×10^{-5} . Fig. 5(B) demonstrates the induced growth in the radius of the trajectory in response to an increment on the deformation amplitude for three different values of $\mu_0 H_z$. The trajectory radius increases linearly with the increment of A_{SAW} up to a certain deformation amplitude. To illustrate this behaviour, we note that for $\mu_0 H_z = 500$ mT the resonance frequency $\omega_G/(2\pi) \simeq 0.75$ GHz is independent on the deformation amplitude for $A_{\text{SAW}} < 25 \times 10^{-5}$. For increased A_{SAW} a resonance frequency shift is observed and the core trajectory is distorted. The open symbols in Fig. 5(B) show that the strain terms cause only a negligible correction in the orbit radius (and only beyond linear regime), meaning that the rotational contribution alone is sufficient to generate stable gyrotropic motion of the vortex core. For that reason, whether the SAWs couple to the gyrotropic mode is determined by the effective magneto-acoustic fields acting on the equilibrium position. The rotation term is capable of shifting the vortex core from the disk's center, but as it rotates around the equilibrium position, the couple of the strain terms averages to zero.

Figure 5(C) shows the dependence of the trajectory radius on the applied perpendicular field, with $A_{\text{SAW}} = 10 \times 10^{-5}$. With this SAW amplitude, the vortex core trajectory is circular in the full range of studied fields. The impact of the perpendicular applied field is to tilt the magnetic moments of the curling in-plane vortex texture out-of-plane in the direction of the field and to slightly enlarge the vortex core

[23, 33]. This out-of-plane tilted vortex structure is called the vortex cone state. One can see that the trajectory radius increases with increased $\mu_0 H_z$. This is a result of the increased rolling field across the full canted structure of the vortex by the increment on the magnetization component along the z -direction, as shown in Fig. 5(D), in contrast to the rather localized rolling field observed for $\mu_0 H_z = 0$ mT [Fig. 5(D) and Fig. 1(D)]. At zero field, the effective field is strictly vanishing outside the vortex core.

Thiele formalism

We now briefly discuss how the tickle and rolling fields, associated with the magneto-elastic and magneto-rotation contributions, respectively [21], drive the vortex core dynamics. Details of the developed formalism are presented in the supplementary material. Within the rigid-core approximation, the magnetization dynamics is captured entirely by the motion of the core in the film plane, whose coordinates are defined by $\mathbf{X} = [X(t), Y(t)]$ which evolve according to the Thiele equation, [15]

$$\mathbf{G} \times \frac{d\mathbf{X}}{dt} + \alpha \mathbf{D} \cdot \frac{d\mathbf{X}}{dt} = -\frac{\partial U}{\partial \mathbf{X}}, \quad (1)$$

where \mathbf{G} is the gyrovector, \mathbf{D} is the damping tensor, and U represents the micromagnetic energy that describes the potential experienced by the vortex core.

For a vortex confined in a thin-film disk in the absence of external driving, this energy is a central potential of the form $U = U_0(\|\mathbf{X}\|^2)$, resulting in damped gyrotropic motion of the vortex core around the disk center. Writing the usual ansatz for the vortex core profile in spherical polar coordinates for the magnetization vector orientation, consider a time-dependent magneto-elastic term,

$$U_{me}(t) = \frac{B_1}{\mu_0 M_s} \int dV \varepsilon_{zz}(t) m_z(\mathbf{r}, t)^2, \quad (2)$$

which results in the tickle field along the z axis

$$h_{\text{tickle}}^z(t) = -\frac{2B_1}{\mu_0 M_s} \varepsilon_{zz}(t) m_z(\mathbf{r}, t). \quad (3)$$

This tickle field acts like an anisotropy field along the z -axis, which can excite magnetization out of the film plane, such as radial spin wave modes of the vortex state [34–37], but does not result in any core dynamics in the limit that the SAW wavelength is much larger than the core. In this case, the integral in Eq. 2 leads to a constant value, independent of the core position, which does not generate a force in Eq. 1, i.e., $\partial U_{me}/\partial X = \partial U_{me}/\partial Y = 0$. Consider now a time-dependent magneto-rotation term,

$$U_{mr}(t) = -M_s \int dV \omega_{xz}(t) m_x(\mathbf{r}, t) m_z(\mathbf{r}, t), \quad (4)$$

which results in the rolling field,

$$h_{\text{roll}}^{x,z}(t) = M_s \omega_{xz}(t) m_{z,x}(\mathbf{r}, t). \quad (5)$$

While this term also generates an effective field along the z direction, proportional to the in-plane magnetization component m_x , it also generates an effective field in the film plane along x that is proportional to the perpendicular magnetization component, m_z . In the long wavelength limit of the SAW, we find the effective magneto-rotation force on the vortex gyration is

$$-\frac{\partial U_{mr}(t)}{\partial X} = 0; \quad -\frac{\partial U_{mr}(t)}{\partial Y} = F_Y(t), \quad (6)$$

which has the same form as the force exerted by an in-plane magnetic field along x . For small displacements of the core, the force at $\mu_0 H_z = 0$ mT can be expressed in terms of the static core profile as

$$F_Y(t) = \pi M_s t_{\text{FM}} \omega_{xz}(t) \int dr \left(r \frac{\partial \Theta_0(r)}{\partial r} \cos 2\Theta_0(r) + \frac{1}{2} \sin 2\Theta_0(r) \right), \quad (7)$$

where t_{FM} is the film thickness. By using the Usov ansatz, the integral can be evaluated to give $F_Y = \pi M_s t_{\text{FM}} \omega_{xz}(t) (1 - \log 2) b$, where b is the core radius, which shows that the magneto-rotation force is proportional to the size of the core. At $\mu_0 H_z > 0$ mT, m_z is nonzero outside the core which increases F_Y .

CONCLUSION

In summary, we demonstrated through a series of experiments that a SAW can excite the vortex gyrotropic mode. The resonant excitation is achieved when the SAW frequency matches the vortex gyrotropic frequency. Thanks to our specific device design we were able to excite the gyrotropic mode either inductively or acoustically, and perform comparative spectroscopy to bring useful insights on the underlying physics. We conclude via micromagnetic simulations that the magneto-rotation coupling is capable of displacing the vortex core from the equilibrium position and inducing a stable gyration. This lifts the requirement for finite magnetostriction, since magneto-rotation coupling is active in all magnets. We observed that the vortex core trajectory increases both with the amplitude of the elastic deformation and, with the amplitude of out-of-plane applied field. In addition, other excitation modes of the vortex ground state exist beside the fundamental gyrotropic mode. The excitation spectrum is composed of radial and azimuthal spin-wave modes developing in the vortex plane. These higher frequency modes may also be excited acoustically and the results presented here will serve as useful input into future investigations.

MATERIALS AND METHODS

Sample

The magnetic stack consists of four layers: Ta(6 nm, buffer)/CoFeB(34 nm)/Ru(0.4 nm)/Ta(3 nm, cap). The CoFeB layer was deposited from from a $\text{Co}_{40}\text{Fe}_{40}\text{B}_{20}$ (at. %) target. The deposition is done at room temperature by dc-magnetron sputtering at pressure of argon of 5×10^{-3} mbar and base pressure below 10^{-7} mbar. The substrate utilized was a Z-cut LiNbO_3 . A post-growth thermal treatment was applied to suppress any magnetic anisotropy [38]. This stack is patterned into disks to have a vortex configuration as magnetic ground state. For this reason, the disks have a diameter $2R = 800$ nm. Additionally, the device includes a broadband microwave antenna of width $w_{\text{ant}} = 4 \mu\text{m}$ designed to generate an in-plane microwave field at the disk's location.

To excite the SAWs, we employ a 5:2 IDT design made of Al(70 nm) with 75-fingers and a finger/interdigit width of $0.9 \mu\text{m}$ (periodicity of $9 \mu\text{m}$). The 1st harmonic order of the IDT is around 0.43 GHz. See the supplementary material for further IDT characterization details. By applying a microwave voltage to the IDT, a periodic elastic deformation is induced in the LiNbO_3 substrate. Notably, the wavelength of the excited SAW is considerably longer than the diameter of the disks under study. Consequently, we assume the strain and the lattice rotation to be spatially uniform across the vortex structure in our modelling.

MRFM

The magnetization dynamics of magnetic disks are detected using MRFM [24]. This technique allows a mechanical detection of the magnetization dynamics through a magnetic probe that is attached to the end of a very soft cantilever. As the magnetization of the disk is excited at resonance, its static component varies, resulting in a change of the dipolar force acting on the magnetic probe. The MRFM signal is an optical detection of the resulting displacement of the cantilever beam. In this study, excitation is induced either by the effective magneto-acoustic field generated by SAWs or by a microwave field generated via an inductive antenna. To improve the signal-to-noise ratio, the excitation field is modulated at the mechanical resonance frequency of the cantilever. More details on the on the sign of the MRFM signal when detecting the dynamics of a magnetic vortex can be found in Ref. [36].

Micromagnetic simulation details

The micromagnetic simulation are performed with Mumax 3 software [31]. The simulated system is a disk of diameter 800 nm and thickness 34 nm, which is divided in $512 \times 512 \times 1$ cells. The material parameters were set corresponding to CoFeB disk as follows: saturation magnetization $M_S = 1.35 \times 10^6$ A/m, exchange stiffness $A_{\text{ex}} = 21$ pJ/m, damping parameter $\alpha = 0.02$. The magnetostrictive character of CoFeB is considered by the magnetic coupling constants $B_1 = B_2 = -8.8$ MJ/m³. In the micromagnetic simulations, we consider a SAW Rayleigh wave in an isotropic substrate. Thus, SAWs travelling along the x -axis can be characterized by the non-vanishing components ϵ_{xx} and ϵ_{zz} of the strain tensor $\epsilon_{ij} = \frac{1}{2} \left(\frac{\partial u_i}{\partial x_j} + \frac{\partial u_j}{\partial x_i} \right)$ and the rotation ω_{xz} . The shear strain ϵ_{xz} exactly vanishes at the surface between the piezoelectric substrate and the magnetic disk. In addition, we assume that the strain in the SAW is transferred entirely to the magnetic disk. The strain components can be implemented as time- and position-dependent excitations in the simulations. Given that the wavelength of the excited SAW is considerably longer than the diameter of the disks we considered the excitation as spatially uniform across the disk. Therefore, the acoustic excitation propagating along the x -axis can be considered by the time-dependent strain tensors as follows,

$$\begin{aligned}
 e_{xx}(t) &= A_{\text{SAW}} \epsilon_{xx} \left(2 \frac{B_1}{M_S} \right) \sin(2\pi ft), \\
 e_{zz}(t) &= A_{\text{SAW}} \epsilon_{zz} \left(2 \frac{B_1}{M_S} \right) \sin(2\pi ft), \\
 e_{xz}(t) &= A_{\text{SAW}} \omega_{xz} (\mu_0 M_S) \sin(2\pi ft + \pi/2), \\
 \epsilon_{yy} &= \epsilon_{yx} = \epsilon_{yz} = 0.
 \end{aligned} \tag{8}$$

Note that the e_{xz} is phase shifted by $\pi/2$ with respect to e_{xx} and e_{zz} . The excitation strength corresponding to magneto-elastic and magneto-rotation contributions are considered by the characteristic fields of $\mu_0 H_{\text{mel}} = 2 \frac{B_1}{M_S} = 11.2$ T and $\mu_0 M_S = 1.7$ T, respectively. The magnetization dynamics in the magnetic disks is simulated for different values of strain amplitudes A_{SAW} and out-of-plane magnetic fields. The vortex core XY coordinates were extracted from the micromagnetic simulations for a given resonance frequency of the gyrotropic mode. We define the trajectory radius by averaging the vortex core distance from the disk center over the last 10 ns seconds of the simulation.

ACKNOWLEDGMENTS

This work was supported by public grants overseen by the French National Research Agency (ANR) as part of the ‘‘Investissements d’Avenir’’ and France 2030 programs (Labex NanoSaclay, reference: ANR-10-LABX-0035, project SPICY. Also: PEPR SPIN, references: ANR 22 EXSP 0008 and ANR 22 EXSP

0004). R. L. S. and F. M. acknowledge the French National Research Agency (ANR) under Contract No. ANR-20-CE24-0025 (MAXSAW).

- [1] M. Weiler, L. Dreher, C. Heeg, H. Huebl, R. Gross, M. S. Brandt, and S. T. Goennenwein, Elastically driven ferromagnetic resonance in nickel thin films, *Physical Review Letters* **106**, [10.1103/PhysRevLett.106.117601](https://doi.org/10.1103/PhysRevLett.106.117601) (2011).
- [2] L. Thevenard, C. Gourdon, J. Y. Prieur, H. J. von Bardeleben, S. Vincent, L. Becerra, L. Largeau, and J.-Y. Duquesne, Surface-acoustic-wave-driven ferromagnetic resonance in (Ga,Mn)(As,P) epilayers, *Phys. Rev. B* **90**, [094401](https://doi.org/10.1103/PhysRevB.90.094401) (2014).
- [3] R. Sasaki, Y. Nii, Y. Iguchi, and Y. Onose, Nonreciprocal propagation of surface acoustic wave in ni/linbo₃, *Phys. Rev. B* **95**, [020407](https://doi.org/10.1103/PhysRevB.95.020407) (2017).
- [4] J. Puebla, M. Xu, B. Rana, K. Yamamoto, S. Maekawa, and Y. Otani, Acoustic ferromagnetic resonance and spin pumping induced by surface acoustic waves, *Journal of Physics D: Applied Physics* **53**, [10.1088/1361-6463/ab7efe](https://doi.org/10.1088/1361-6463/ab7efe) (2020).
- [5] P. Delsing, A. N. Cleland, M. J. A. Schuetz, J. Knörzer, G. Giedke, J. I. Cirac, K. Srinivasan, M. Wu, K. C. Balram, C. Bäuerle, T. Meunier, C. J. B. Ford, P. V. Santos, E. Cerda-Méndez, H. Wang, H. J. Krenner, E. D. S. Nysten, M. Weiß, G. R. Nash, L. Thevenard, C. Gourdon, P. Rovillain, M. Marangolo, J.-Y. Duquesne, G. Fischerauer, W. Ruile, A. Reiner, B. Paschke, D. Denysenko, D. Volkmer, A. Wixforth, H. Bruus, M. Wiklund, J. Reboud, J. M. Cooper, Y. Fu, M. S. Brugger, F. Rehfeldt, and C. Westerhausen, The 2019 surface acoustic waves roadmap, *Journal of Physics D: Applied Physics* **52**, [353001](https://doi.org/10.1088/1361-6463/ab7efe) (2019).
- [6] R. Verba, V. Tiberkevich, and A. Slavin, Wide-band nonreciprocity of surface acoustic waves induced by magnetoelastic coupling with a synthetic antiferromagnet, *Phys. Rev. Appl.* **12**, [054061](https://doi.org/10.1103/PhysRevApplied.12.054061) (2019).
- [7] A. Hernández-Mínguez, F. Macià, J. M. Hernández, J. Herfort, and P. V. Santos, Large nonreciprocal propagation of surface acoustic waves in epitaxial ferromagnetic/semiconductor hybrid structures, *Physical Review Applied* **13**, [10.1103/PhysRevApplied.13.044018](https://doi.org/10.1103/PhysRevApplied.13.044018) (2020).
- [8] M. Xu, K. Yamamoto, J. Puebla, K. Baumgaertl, B. Rana, K. Miura, H. Takahashi, D. Grundler, S. Maekawa, and Y. Otani, Nonreciprocal surface acoustic wave propagation via magneto-rotation coupling, *Sci. Adv.* **6**, <https://doi.org/10.1126/sciadv.abb1724> (2020).
- [9] F. Millo, J.-P. Adam, C. Chappert, J.-V. Kim, A. Mouhoub, A. Solognac, and T. Devolder, Unidirectionality of spin waves in synthetic antiferromagnets, *Phys. Rev. Appl.* **20**, [054051](https://doi.org/10.1103/PhysRevApplied.20.054051) (2023).
- [10] M. Küß, S. Glamsch, A. Hörner, and M. Albrecht, Wide-band nonreciprocal transmission of surface acoustic waves in synthetic antiferromagnets, *ACS Appl. Electron. Mater.* (2024).
- [11] R. Sasaki, Y. Nii, and Y. Onose, Surface acoustic wave coupled to magnetic resonance on multiferroic cub₂O₄, *Phys. Rev. B* **99**, [014418](https://doi.org/10.1103/PhysRevB.99.014418) (2019).

- [12] H. Matsumoto, T. Kawada, M. Ishibashi, M. Kawaguchi, and M. Hayashi, Large surface acoustic wave nonreciprocity in synthetic antiferromagnets, *Applied Physics Express* **15**, 063003 (2022).
- [13] T. P. Lyons, J. Puebla, K. Yamamoto, R. S. Deacon, Y. Hwang, K. Ishibashi, S. Maekawa, and Y. Otani, Acoustically driven magnon-phonon coupling in a layered antiferromagnet, *Phys. Rev. Lett.* **131**, 196701 (2023).
- [14] R. P. Cowburn, D. K. Koltsov, A. O. Adeyeye, M. E. Welland, and D. M. Tricker, Single-domain circular nanomagnets, *Phys. Rev. Lett.* **83**, 1042 (1999).
- [15] K. Y. Guslienko, Magnetic vortex state stability, reversal and dynamics in restricted geometries, *Journal of Nanoscience and Nanotechnology* **8**, 2745 (2008).
- [16] V. Novosad, F. Y. Fradin, P. E. Roy, K. S. Buchanan, K. Y. Guslienko, and S. D. Bader, Magnetic vortex resonance in patterned ferromagnetic dots, *Phys. Rev. B* **72**, 024455 (2005).
- [17] S. Kasai, Y. Nakatani, K. Kobayashi, H. Kohno, and T. Ono, Current-driven resonant excitation of magnetic vortices, *Phys. Rev. Lett.* **97**, 107204 (2006).
- [18] V. S. Pribiag, I. N. Krivorotov, G. D. Fuchs, P. M. Braganca, O. Ozatay, J. C. Sankey, D. C. Ralph, and R. A. Buhrman, Magnetic vortex oscillator driven by d.c. spin-polarized current, *Nature Physics* **3**, 498 (2007).
- [19] A. Koujok, A. Riveros, D. R. Rodrigues, G. Finocchio, M. Weiler, A. Hamadeh, and P. Pirro, Resonant excitation of vortex gyrotropic mode via surface acoustic waves, *Applied Physics Letters* **123**, 132403 (2023).
- [20] K. Yamamoto and S. Maekawa, Magnetostatic field induced by mechanical deformations, *Annalen der Physik* **536**, 2300395 (2024).
- [21] R. Lopes Seeger, L. La Spina, V. Laude, F. Millo, A. Bartaszyte, S. Margueron, A. Solignac, G. de Loubens, L. Thevenard, C. Gourdon, C. Chappert, and T. Devolder, Symmetry of the coupling between surface acoustic waves and spin waves in synthetic antiferromagnets, *Phys. Rev. B* **109**, 104416 (2024).
- [22] S. Maekawa and M. Tachiki, Surface acoustic attenuation due to surface spin wave in ferro- and antiferromagnets, *AIP Conference Proceedings* **29**, 542 (1976).
- [23] G. de Loubens, A. Riegler, B. Pigeau, F. Lochner, F. Boust, K. Y. Guslienko, H. Hurdequint, L. W. Molenkamp, G. Schmidt, A. N. Slavin, V. S. Tiberkevich, N. Vukadinovic, and O. Klein, Bistability of vortex core dynamics in a single perpendicularly magnetized nanodisk, *Physical Review Letters* **102**, 177602 (2009).
- [24] O. Klein, G. de Loubens, V. V. Naletov, F. Boust, T. Guillet, H. Hurdequint, A. Leksikov, A. N. Slavin, V. S. Tiberkevich, and N. Vukadinovic, Ferromagnetic resonance force spectroscopy of individual submicron-size samples, *Phys. Rev. B* **78**, 144410 (2008).
- [25] R. L. Compton and P. A. Crowell, Dynamics of a pinned magnetic vortex, *Phys. Rev. Lett.* **97**, 137202 (2006).
- [26] S. Shreya, A. S. Jenkins, Y. Rezaeiyan, R. Li, T. Böhnert, L. Benetti, R. Ferreira, F. Moradi, and H. Farkhani, Granular vortex spin-torque nano oscillator for reservoir computing, *Scientific Reports* **13**, 16722 (2023).
- [27] K. An, A. N. Litvinenko, R. Kohno, A. A. Fuad, V. V. Naletov, L. Vila, U. Ebels, G. de Loubens, H. Hurdequint, N. Beaulieu, J. Ben Youssef, N. Vukadinovic, G. E. W. Bauer, A. N. Slavin, V. S. Tiberkevich, and O. Klein, Coherent long-range transfer of angular momentum between magnon kittel modes by phonons, *Phys. Rev. B* **101**, 060407 (2020).

- [28] B. Casals, N. Statuto, M. Foerster, A. Hernández-Mínguez, R. Cichelero, P. Manshausen, A. Mandziak, L. Aballe, J. M. Hernández, and F. Macià, Generation and imaging of magnetoacoustic waves over millimeter distances, *Phys. Rev. Lett.* **124**, 137202 (2020).
- [29] B. Pigeau, G. de Loubens, O. Klein, A. Riegler, F. Lochner, G. Schmidt, L. W. Molenkamp, V. S. Tiberkevich, and A. N. Slavin, A frequency-controlled magnetic vortex memory, *Applied Physics Letters* **96**, 132506 (2010), https://pubs.aip.org/aip/apl/article-pdf/doi/10.1063/1.3373833/14432797/132506_1_online.pdf.
- [30] A. Drews, B. Krüger, G. Selke, T. Kamionka, A. Vogel, M. Martens, U. Merkt, D. Möller, and G. Meier, Nonlinear magnetic vortex gyration, *Phys. Rev. B* **85**, 144417 (2012).
- [31] A. Vansteenkiste, J. Leliaert, M. Dvornik, M. Helsen, F. Garcia-Sanchez, and B. Van Waeyenberge, The design and verification of MuMax3, *AIP Advances* **4**, 107133 (2014).
- [32] V. Iurchuk, J. Lindner, J. Fassbender, and A. Kákay, Excitation of the gyrotropic mode in a magnetic vortex by time-varying strain (2023), [arXiv:2311.18517](https://arxiv.org/abs/2311.18517) [physics.app-ph].
- [33] B. A. Ivanov and G. M. Wysin, Magnon modes for a circular two-dimensional easy-plane ferromagnet in the cone state, *Phys. Rev. B* **65**, 134434 (2002).
- [34] B. A. Ivanov and C. E. Zaspel, High frequency modes in vortex-state nanomagnets, *Phys. Rev. Lett.* **94**, 027205 (2005).
- [35] K. Vogt, O. Sukhostavets, H. Schultheiss, B. Obry, P. Pirro, A. A. Serga, T. Sebastian, J. Gonzalez, K. Y. Guslienko, and B. Hillebrands, Optical detection of vortex spin-wave eigenmodes in microstructured ferromagnetic disks, *Phys. Rev. B* **84**, 174401 (2011).
- [36] V. Castel, J. Ben Youssef, F. Boust, R. Weil, B. Pigeau, G. de Loubens, V. V. Naletov, O. Klein, and N. Vukadinovic, Perpendicular ferromagnetic resonance in soft cylindrical elements: Vortex and saturated states, *Phys. Rev. B* **85**, 184419 (2012).
- [37] B. Taurel, T. Valet, V. V. Naletov, N. Vukadinovic, G. de Loubens, and O. Klein, Complete mapping of the spin-wave spectrum in a vortex-state nanodisk, *Physical Review B* **93**, 184427 (2016).
- [38] R. L. Seeger, F. Millo, A. Mouhoub, G. de Loubens, A. Solignac, and T. Devolder, Inducing or suppressing the anisotropy in multilayers based on cofeb, *Phys. Rev. Mater.* **7**, 054409 (2023).